**Article:**
Yang, K., Rongong, J.A. and Worden, K. (2018) Damage detection in a laboratory wind turbine blade using techniques of ultrasonic NDT and SHM. Strain, 54 (6). e12290. ISSN: 0039-2103

https://doi.org/10.1111/str.12290

# Damage Detection in a Laboratory Wind Turbine Blade using Techniques of Ultrasonic NDT and SHM

**K. Yang**[a], **J.A. Rongong**[b] and **K. Worden**[b1]

[a]TWI Ltd, Granta Park, Cambridge CB21 6AL, UK

[b]Dynamics Research Group, Department of Mechanical Engineering, University of Sheffield, Mappin Street, Sheffield S1 3JD, UK

## Abstract

This paper presents a case study in the use of ultrasonic NDE/SHM techniques for detecting and locating damage in a real (but small) wind turbine blade. Two techniques are considered: (i) nonlinear acoustics, and (ii) guided-wave 'pitch-catch' SHM. While the nonlinear acoustics approach proved disappointingly insensitive to damage induced experimentally in the blade, the guided-wave approach not only detected the damage, but proved capable of locating it, using a 'network of novelty detectors' methodology. A first, slightly ill-conceived, programme of guided-wave tests actually provided valuable insight into attenuation of waves in the structure of interest and supported the idea that actuator-sensor networks of a feasible density could be used for wind turbine blade SHM.

**Key words:** Structural Health Monitoring (SHM); wind turbine blades; nonlinear acoustics; guided wave-based SHM.

## 1 Introduction

This paper presents the final part of the research conducted for the PhD project [1]. The overall project was concerned with comparing a number of ultrasonic methods for the detection of damage in various coupons and structures. The methods investigated included vibro-acoustic techniques, nonlinear acoustics, and guided-wave structural health monitoring (SHM). Previously published work reported results on glass [2] and composite specimens [3]. As shown in the thesis [1], all the methods considered proved capable of detecting fatigue cracks in the glass and composite coupons. For the final study, it was decided to test a more challenging structure. A small (but real) wind turbine (WT) blade was chosen as the structure of interest.

There were two major reasons for choosing a WT blade; the first was because of the current importance of wind turbines in meeting renewable energy targets for the future. Wind is a clean source of renewable energy that has been used for more than a thousand years. The most typical example is the windmill that converts wind energy to rotational energy. Since the growing fossil fuel crisis started in the 1970s, energy prices have increased dramatically [4]. In addition, global environmental issues have attracted considerable attention. As a response to environmental threats and rising energy prices, commercial wind turbines were introduced in 1980 [5]. In general, a wind turbine converts the kinetic energy of wind into electrical energy [6, 7]. As mentioned by Jha [7], a wind turbine is designed for producing industrially useful amounts of energy with eco-friendly effects, compared to other energy resources. However, the operation and maintenance costs of a wind turbine cannot be ignored. According to Verbruggens research [8], the operation and maintenance costs take up 30%-35% of the total electricity costs from a wind turbine. One effective way forward is to reduce the life cycle costs and to extend the life of the wind turbine structure by the application of SHM.

The second reason for the choice of structure here relates to a serious issue in the application of ultrasonic wave-based SHM to WT blades. WT blades are very large structures, with current generations of blades approaching 100 m in length. Furthermore, blades are typically manufactured from composite materials which are known to have high levels of attenuation for ultrasonic

[1]Corresponding Author: k.worden@sheffield.ac.uk

waves. Clearly a limitation of the use of guided-wave SHM is the density of the sensor/actuator network needed; if too high a sensor/actuator density is needed, then ultrasonic SHM is infeasible. This project allowed an investigation into the degree of attenuation experienced by a guided-wave SHM system implemented on a structure manufactured from realistic material.

Another difference in the current study, was the damage mechanism investigated. In [2, 3], single fatigue cracks were initiated and propagated in the glass and composite plates under fairly ideal laboratory fatigue test conditions. In the current study, it was decided to generate the damage via a more realistic mechanism. It is widely accepted that fibre-reinforced polymer-based wind turbine blades are susceptible to *low velocity impact damage* e.g. from hail or birdstrike. The low velocity impact often causes internal damage and is usually barely detectable by eye. This damage although small, may propagate to more severe damage and eventually cause failure of the structure without warning. The damage in the WT blade of this study was generated using a hammer impact.

In summary, this paper presents damage detection on an wind turbine blade exposed to impact, by using modal analysis, nonlinear acoustics and guided-wave SHM. The layout of the paper is as follows. Section Two presents the results of an experimental modal analysis of the WT blade; this provided useful information in designing the subsequent programme of SHM activity. Section Three presents the experimental programme and results based on nonlinear acoustics, while Section Four does the same for the guided wave-based SHM approach. The paper ends with some discussion and conclusions.

## 2 Experimental Modal Analysis of the Wind Turbine Blade

The structure under consideration is a Skystream 3.7 wind turbine blade; this is a small WT, rated at 2.4 kW nominal power, designed and intended for personal use. It has a cut-in wind speed of 3.5 m/s and a rated speed of 9 m/s. The blade has a total length of 1.8 m and weighs 5.5 kg; it is made out of fibre-reinforced polymer. Modal analysis was required for the blade in order to design the nonlinear acoustics tests described later. In the nonlinear acoustic tests, the blade is excited at a low-frequency mode (to generate 'high' amplitude response) at the same time as an ultrasonic excitation is applied. For this reason, it is important to understand the modal properties of the blade e.g. what the natural frequencies of the vibrations modes are, and where the nodes of the corresponding mode shapes are.

The structure was clamped at its base, to a substantial frame with four M10 bolts given a torque of 50Nm; this gave fixed-free (cantilever) boundary conditions (Figure 1). For the modal tests, the blade was excited using an LDS VS406 electromagnetic shaker attached to the lower part of the blade through a thin stinger, such that the force was applied perpendicular to the blade surface. The blade response was measured using unidirectional piezoelectric accelerometers, and a standard piezoelectric force transducer was used to record the excitation force. All data acquisition was accomplished using an LMS SCADAS III.

A schematic showing the position of the 26 accelerometers used to measure the dynamic responses is shown in Figure 2

Figure 3 shows a typical Frequency Response Function (FRF) estimated from the structure. Random excitation was used with a frequency bandwidth of 0 – 1024 Hz and a frequency resolution of 0.125 Hz. The $H_v$ FRF estimator was used. The Polymax modal parameter estimation algorithm was used for the extraction of the natural frequencies and mode shapes of the blade; the first ten natural frequencies are presented in Table 1.

For this study, the $4^{th}$ vibration mode ($3^{rd}$ bending mode) was initially selected as being suitable for the low-frequency excitation. The mode shape for the $4^{th}$ vibration mode is shown in Figure 4; the eigen-frequency for the mode is 71.5 Hz.

Based on the mode shape of the blade i.e. the positions of nodes and antinodes, a number of low-frequency excitation points were allocated on the blade. In order to mitigate the effect of wave energy dissipation over 'long' distances, the blade was divided into four sections, with each section allocated a piezoelectric stack actuator (PI ceramic PL-055.31) for low-frequency

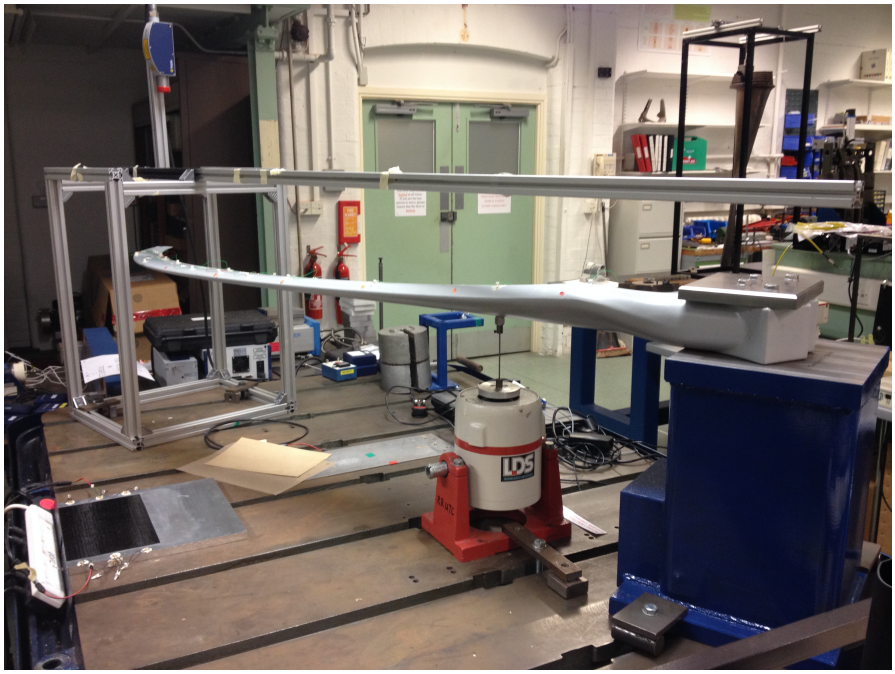

Figure 1: The experimental configuration of the WT blade, showing the geometric boundary conditions.

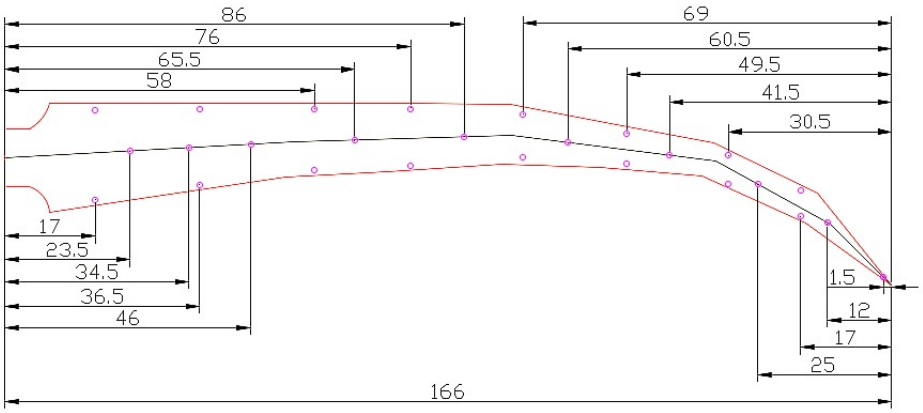


Figure 2: The distribution of the 26 measurement points on the testing blade. The circles mark the accelerometer locations. The unit of length is the centimetre

excitation. The stack actuator geometries used were the same as those used in the previous studies on plates and coupons [2, 3, 1]. An HBM-X60 2-component fast-curing glue was used to attach the stack actuators which were additionally amplified to the required level with a PI E-505 LVPZT piezo-amplifier. The orientation of each stack actuator is locally out-of-plane. In addition, four PZTs (PI ceramic PIC155 transducers) around the centre stack actuator were employed for sensing and actuation of high-frequency signals. The placement of the actuators and sensors is shown schematically in Figure 5.

In order to excite the blade when it was initially tested in its intact condition, a swept-sine signal, starting at 1Hz and increasing up to 500Hz over a period of 2s was used. However, it was found that the dynamic response for the $4^{th}$ vibration mode was not as strong as anticipated when the swept-sine signals were applied at positions I, III and IV, as these were still too close to nodal points and constraints. Although 71.5 Hz was clearly not an ideal excitation frequency

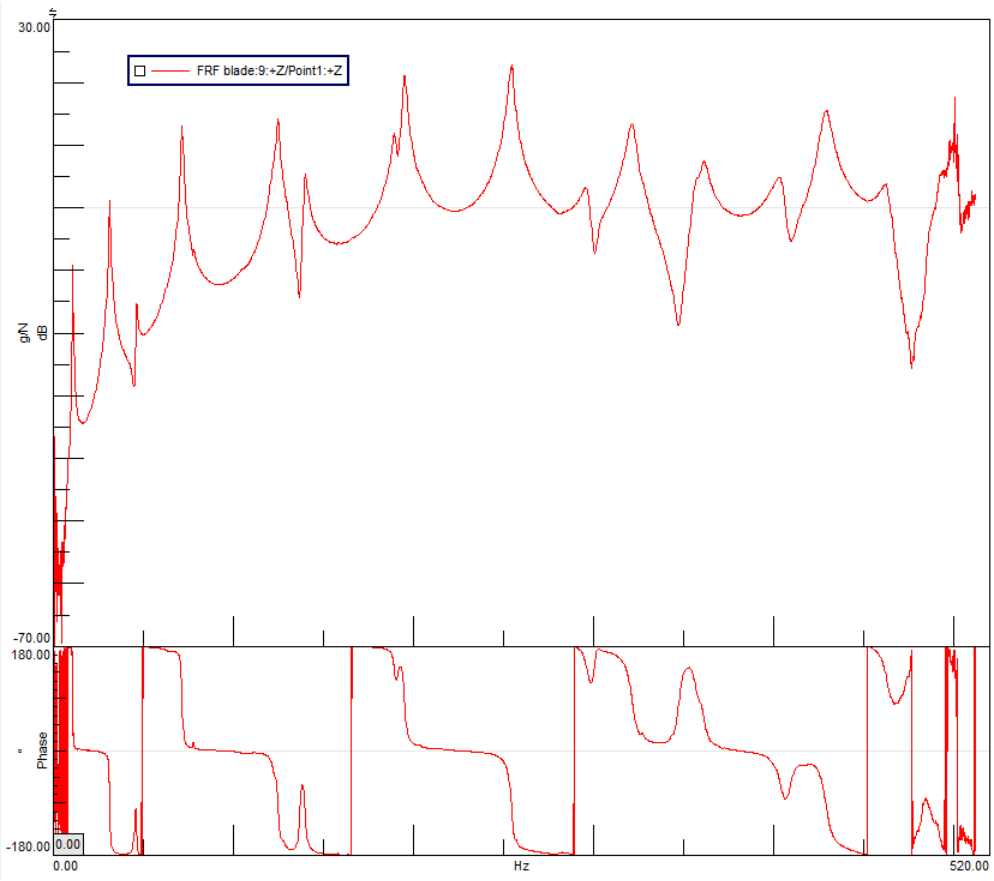


Figure 3: Plot of Extracted FRF from modal analysis.

| Mode | Natural Frequency (Hz) |
|---|---|
| 1 | 10.5 |
| 2 | 31.0 |
| 3 | 45.6 |
| 4 | 71.5 |
| 5 | 124.5 |
| 6 | 140.4 |
| 7 | 195.3 |
| 8 | 254.2 |
| 9 | 279.5 |
| 10 | 320.0 |

Table 1: The first ten natural frequencies of the WT blade, as measured by the LMS system.

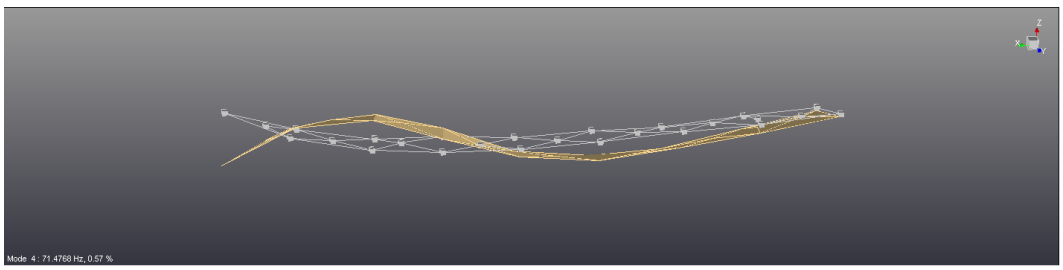

Figure 4: $4^{th}$ vibration mode obtained by LMS system. The gray (dotted) frame lines represent the undeformed states.

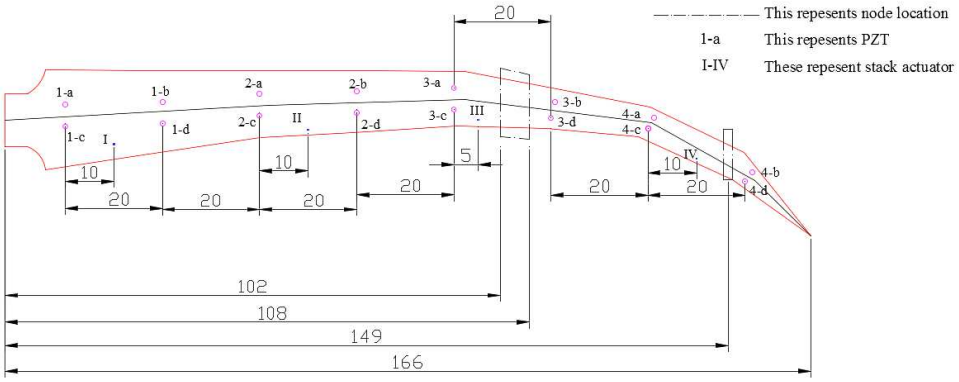


Figure 5: Schematic of the location of the sensors. The red circles represent the PZTs. The Roman numerals represent the stack actuators. The dash dot line areas manifest the nodal locations. The unit of length is the centimetre

at positions I, III and IV, it was established that other vibration modes could also be excited adequately at these positions, e.g. the $8^{th}$ vibration mode (257.5Hz) for position I, $6^{th}$ mode (141.2Hz) for position III, and the $10^{th}$ mode (308.6Hz) for position III. The mode shapes for these three modes are shown in Figure 6.

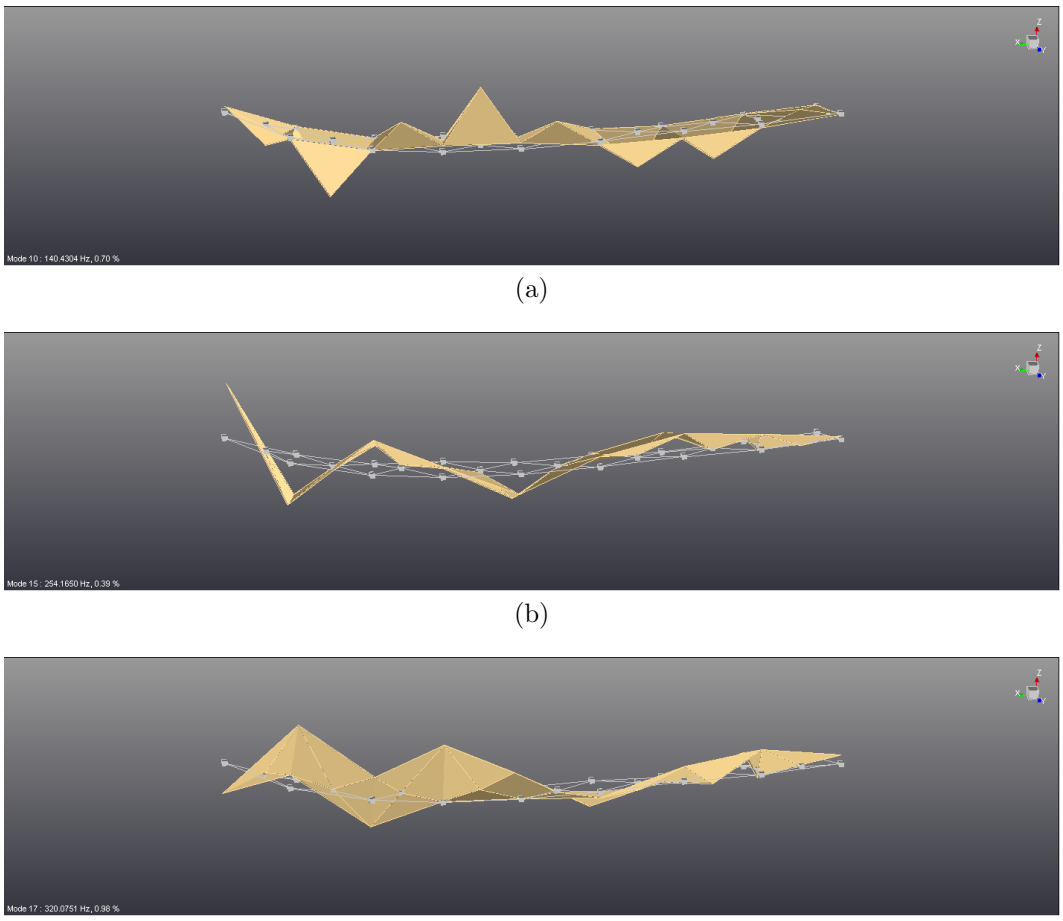

(a)

(b)

(c)

Figure 6: WT blade vibration mode shapes for: (a) the $6^{th}$ mode, (b) $8^{th}$ mode and, (c) $10^{th}$ mode. The gray frame lines represent the undeformed states.

Having determined appropriate positions for the stack actuators and identified the best modal frequencies for low-frequency actuation, the experimental programme moved to the nonlinear acoustic tests.

# 3 Nonlinear Acoustic Tests

The basic idea of the nonlinear acoustic tests is as follows. If damage is present within a structure, and that structure is excited with two different frequencies $f_1$ and $f_2$, nonlinearity induced by the damage will generate higher-order harmonics of both excitation frequencies which will cause the response to contain 'combination' frequencies e.g. $f_1 \pm f_2$, $f_1 + 2f_2$, $2f_1 + f_2$ etc. If the structure is undamaged, and linear, the combination frequencies can not appear, and therefore their presence can be interpreted as a signature of damage. A convenient way to implement the test is to make the frequency $f_1$ low, corresponding to a structural mode (in order to generate high amplitude response), and to make $f_2$ high, usually in the ultrasonic range. Under these conditions, the combination frequencies will appear as sidebands around $f_2$ with a spacing of $f_1$. Estimation of the severity of the nonlinearity (and thus the damage) can then be carried out by estimating the energy in the sidebands. This very brief discussion does not even scratch the surface of the subject, which was initiated in the 1960s when it was considered as a means of detecting material defects [9]. (A comparatively recent review on assessment of micro-damage using nonlinear acoustics can be found in [10]). The technique began to see applications in NDT/NDE towards the end of the twentieth century, [11] is a typical reference, and attracted attention in the SHM field around a decade later (see e.g. [12, 13]).

In fact, nonlinear acoustics can be implemented with a single frequency $f_1$ excitation, as nonlinearity will potentially create reponses at harmonics of the base frequency i.e. $2f_1$, $3f_1$, $4f_1$ etc. The problem in practice, is that any nonlinearity present in the measurement chain can also cause the presence of harmonics and/or combination frequencies. For this reason, it is usual to carry out a baseline test on the structure of interest when it is known to be undamaged, in order to assess the 'background' level of nonlinearity; damage might later be inferred if the effects of nonlinearity show a statistically significant departure from the baseline level.

## 3.1 Experimental Procedure

The low- and high-frequency excitation signals were generated using a two-channel TTi-TGA 1242, 40 MHz arbitrary waveform generator. The low-frequency signal driving the stack actuator was further amplified to the required level with a PI E-505 LVPZT piezo-amplifier. Signal responses were acquired using a four-channel LeCroy Waverunner LT264, 350 MHz, 1 GS/s digital oscilloscope.

The tests were carried out in four stages geometrically, section by section using the single stack actuator relevant to the section (Figure 5). In each case the low-frequency excitation corresponded to a natural frequency: Section 1/stack I – vibration mode 4 – 71.5 Hz; Section 2/stack II – vibration mode 8 – 257,5 Hz; Section 3/stack III – vibration mode 6 – 141.2 Hz; Section 4/stack IV – vibration mode 10 – 308.6 Hz. The arrangements of the stacks and the high-frequency actuators and sensors are shown in Figure 7. Each stage of the test sequence used two methodologies; in the first case, a single frequency of excitation was applied in order to estimate whether energy was transferred into harmonics; in the second case, both low- and high frequency excitations were applied in order to estimate how much energy was transferred into sidebands.

The first set of tests were carried out on the undamaged blade; the second set on the damaged blade. A single (uncontrolled) blow with an impact hammer (Model: 086D20 – integrated with PCB piezotronics) was used to produce the impact damage and record the contact force. The target strike area is shown in Figure 8. During the impact, the test blade was only constrained at the root and there was no support underneath the strike area. The contact force was recorded as 2247.3 N. As no facilities for C-scan were available, it was not possible to verify the extent of damage caused by the impact, following the tests. At the time, some immediate post-impact damage was visible on the surface of the blade in the form of marks/indentations.

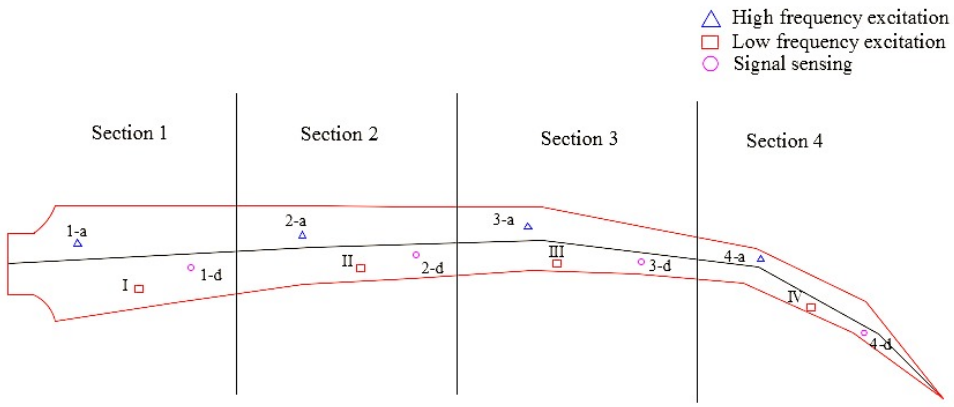


Figure 7: The arrangement of sensors. Blue triangle represents a high frequency excitation transducer. Red rectangle represents a stack actuator. Pink circle represents a receiving sensor.

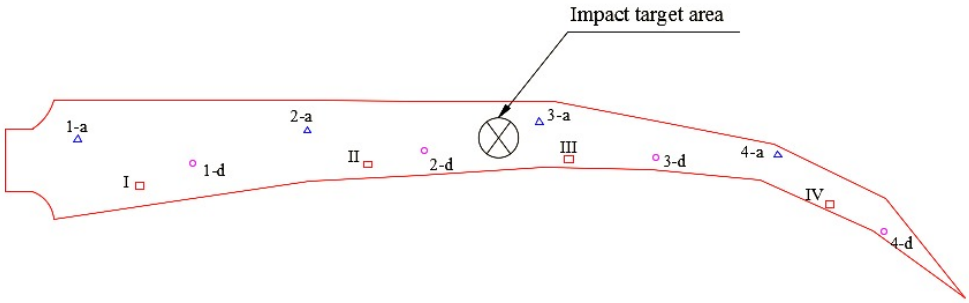


Figure 8: The impact target area.

## 3.2 Analysis and Results

The first set of tests analysed here is the one based on single-frequency excitation. For these tests, the sampling rate for data acquisition was 20 kHz. Figure 9 shows examples of power spectra from the single-wave excitation tests using the $8^{th}$, $4^{th}$, $6^{th}$ and $10^{th}$ vibration modes for test sections 1, 2, 3 and 4, respectively. Results from two different blade conditions are shown, i.e. for the intact blade and the impact-damaged blade. A clear pattern of higher harmonics (second and third) can be observed in all the analysed spectra, even for the undamaged blade (which represents the baseline state for the measurement chain). Unfortunately, there do not appear to be significant differences between the spectra for the undamaged and damaged states, and this does not bode well for the quantitative analysis.

As discussed at the beginning of the section, the analysis is carried out by estimating the 'energy' in the harmonics or sidebands of the response and then determining if there is a statistically significant increase after the damage is imposed. The assessment of significance is carried out via a hypothesis test. A number of features can be used to represent the level of nonlinear distortion, the one used in this analysis is a *perturbation coefficient* $\beta$, which is essentially an appropriately normalised measure of the amplitude of the second harmonic $A_2$ in the response, at a distance $x$ from a source of single frequency $\Omega$ [14],

$$\beta = \frac{8c^2}{\Omega^2 x}\left(\frac{A_2}{A_1^2}\right) \tag{1}$$

where $A_1$ is the amplitude of the fundamental component of the response, and $c$ is the wave speed.

In order to detect damage, one has to show that the $\beta$ coefficient is significantly greater (statistically) for the damage case compared to the baseline case. In order to do this, one uses

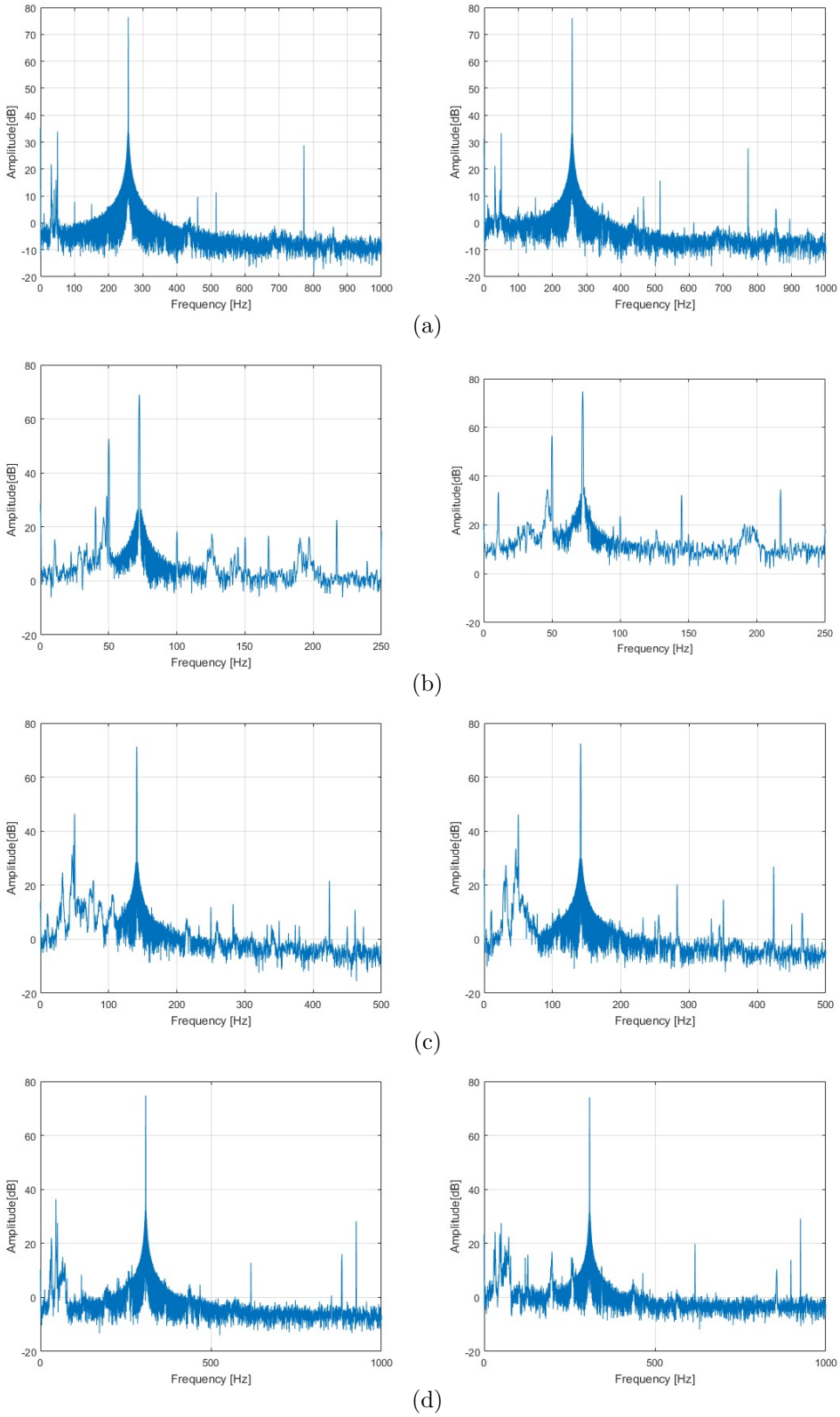


Figure 9: Power spectra density showing the fundamental peak and harmonics for the intact (left column) and impact (right column) blade excited by (a) $8^{th}$ vibration mode for Section 1, (b) $4^{th}$ vibration mode for Section 2, (c) $6^{th}$ vibration mode for Section 3 and (d) $10^{th}$ vibration mode for Section 4.

a hypothesis test based on *small sample statistics* [15]. One wishes to choose between a null hypothesis $H_0$, which in this case corresponds to the case that there is no damage, and therefore that $\beta = 0$, and an alternative hypothesis $H_1$, which is that damage is present and $\beta \neq 0$. In the first test, one assumes that the experimental measurements of $\beta$ will be drawn from a Gaussian probability distribution with mean $\mu_1$ and variance $S_1^2$; in the second test, one assumes that the estimated $\beta$ will be a sample from a Gaussian with mean $\mu_2$ and variance $S_2^2$. One computes a test statistic; as the two sample distributions are Gaussian, the test statistic is $t$-distributed [16]. One estimates the means $\overline{\beta}_1$ and $\overline{\beta}_2$ from samples of size $N_1$ and $N_2$ (before and after potential damage), the test statistic is then,

$$t = \frac{(\overline{\beta}_1 - \overline{\beta}_2) - (\mu_1 - \mu_2)}{\sqrt{\frac{S_1^2}{N_1} - \frac{S_2^2}{N_2}}} \tag{2}$$

Assuming the null hypothesis is that damage has not occurred, then one has that $\mu_1 = \mu_2 = 0$. Furthermore, if one estimates $\beta$ using samples of the same size in tests one and two, so that $N_1 = N_2 = N$, one has,

$$t = \frac{(\overline{\beta}_1 - \overline{\beta}_2)}{\sqrt{\frac{S_1^2 - S_2^2}{N}}} \tag{3}$$

which is $t$-distributed with $N - 1$ degrees of freedom. The null hypothesis is rejected (damage is inferred) if the $t$ sample is beyond some appropriate centile in the right tail of the $t$-distribution. The centile chosen is thus a threshold for damage detection, corresponding to some level of confidence. In the results presented here, the critical value (threshold) corresponds to 95% confidence, and $N = 19$ samples of $\beta$ were used to estimate sample statistics.

Figure 10 shows the test statistic value for the perturbation coefficient $\beta$ against the impact energy (essentially 'no impact' versus 'impact' in this case). Any test statistic value above the critical value line is considered as significant nonlinearity resulting from damage. The results are somewhat disappointing; a statistically significant result is only found for the $4^{th}$ vibration mode for Section 2 (Figure 10b).

The second set of results presented here are for the case when both low- and high frequency excitations were applied. In this case, the sampling frequency for data acquisition was set at 500 kHz. The zoomed power spectra shown in Figure 11 reveal that sidebands are present in the response around the high frequency, and that the frequency spacing of sidebands does indeed correspond to the low-frequency modal excitation, as one might expect. Unfortunately, although some sidebands can be observed for both the undamaged blade and damaged blade, there is no significant change after the impact. In the case of the $4^{th}$ vibration mode, which had shown to be a disappointing choice of excitation for Section 2, there are no visible sidebands.

For the quantitative analysis in this case, the amplitude of the carrier fundamental ultrasonic frequency and the first two pairs of sidebands was used to calculate the *intensity of modulation parameter* $R$,

$$R = \frac{A_1 + A_2}{A_0} \tag{4}$$

where $A_0$ is the magnitude of the High Frequency (HF) ultrasonic component, while $A_1$ and $A_2$ are the magnitudes of the first pair (left and right) of modulation sidebands. For the tests and analysis here, the values for various amplitude levels of LF vibration excitation were used for sample data for a hypothesis test. As the null hypothesis is once again $R = 0$, the same steps as before can be applied in the hypothesis test. Unfortunately, as Figure 12 shows, the test statistic values for all the sections are below threshold. This means the results do not show statistically significant detection of damage, in the current study. This is a disappointment; the nonlinear acoustic features proved capable of detecting damage in the glass and composite specimens in [1]. One reason for this failure could be the level of low-frequency excitation that the stack actuators provided. These were oriented out-of-plane; when excited using an oscillating voltage signal, the stacks stretched and contracted perpendicular to the surface. The blade was thus excited by

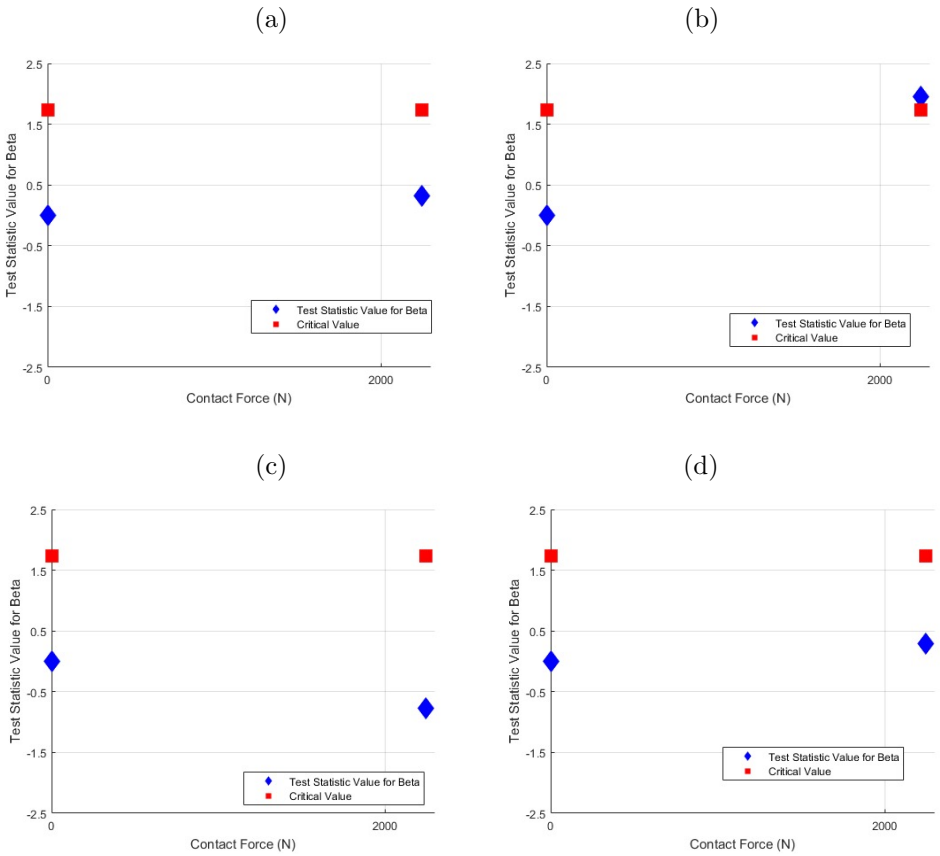


Figure 10: Test statistic value $\beta$ obtained from: (a) $8^{th}$ vibration mode for Section 1; (b) $4^{th}$ vibration mode for Section 2; (c) $6^{th}$ vibration mode for Section 3; (d) $10^{th}$ vibration mode for Section 4. The first point in each graph (Contact Force = 0 N), corresponds to the undamaged state of the blade; the second point (Contact Force 2247.3 N), corresponds to the impact damaged state.

the reaction force resulting from accelerating the actuator. The magnitude of this force can be estimated by considering the mass and maximum stroke of the actuator. The absolute mass of the actuator is 0.38 grams. Assuming linear extension, equivalent kinetic energy indicates that the effective mass is 0.13 grams. The maximum extension of the actuator is 2.2 micrometres. Hence the maximum out-of-plane force than can be generated is (in milli-Newtons):

Mode 4: 0.06; Mode 6: 0.22; Mode 8: 0.73; Mode 10: 1.16;

With the benefit of hindsight, while these small forces were adequate to excite a thin plate, they were insufficient to create meaningful motion on the blade itself. In fact, the nonlinear acoustic tests were not a complete failure. As observed earlier, the damage was detected using the $4^{th}$ vibration mode using the stack actuator for Section 2. As this actuator for Section 2, is one of the two closest to the impact point, the successful detection result may support the conclusion that the problem was a matter of generating sufficient low-frequency vibration energy in the region of the damage. However, one should not conclude that making the nonlinear acoustics approach work in reality is simply a matter of increasing the power of the stack actuator; one should bear in mind that the blade in this study is still very small compared to the vast majority of blades used for large-scale renewable energy generation.

In the next section, a more conventional ultrasonic wave-based SHM approach is followed.

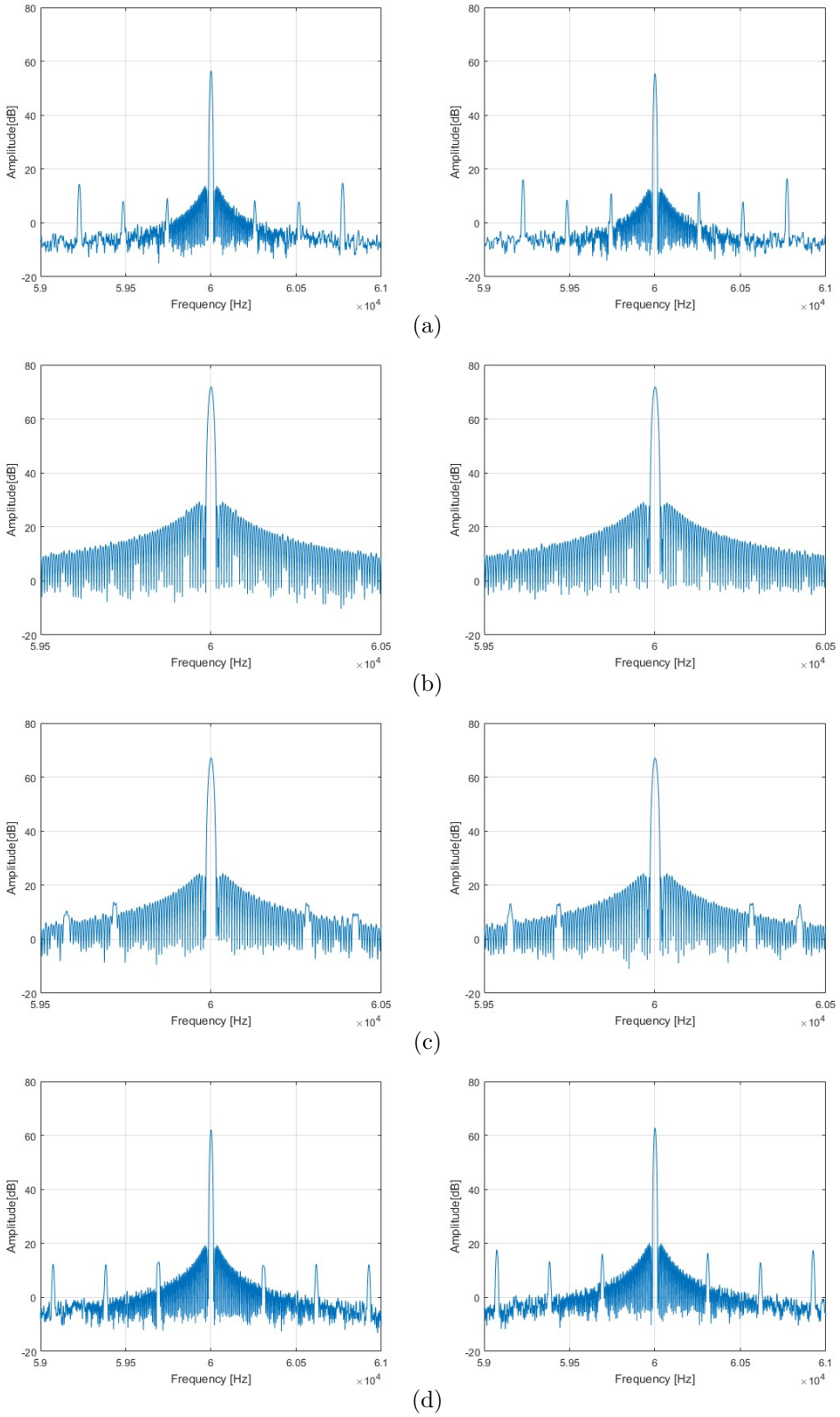


Figure 11: Zoomed power spectra from vibro-acoustic excitation tests using (a) $8^{th}$ vibration mode for Section 1, (b) $4^{th}$ vibration mode for Section 2, (c) $6^{th}$ vibration mode for Section 3 and (d) $10^{th}$ vibration mode for Section 4. Left column: intact blade; right column: impact test blade.

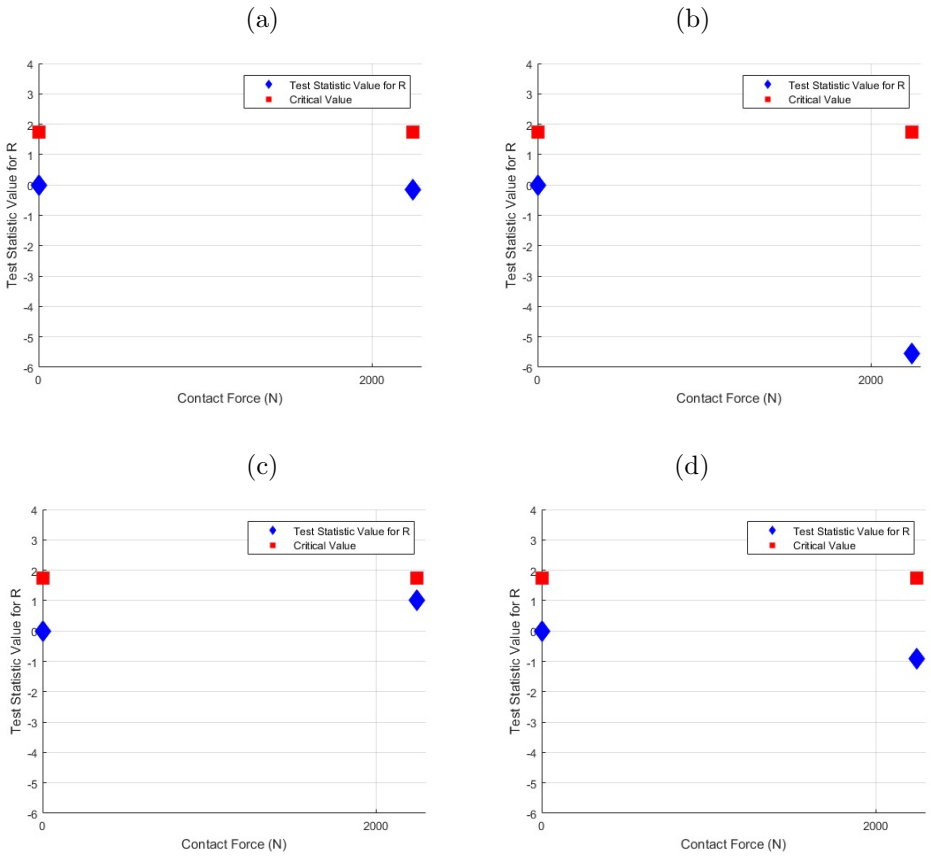


Figure 12: Test statistic value obtained from the vibro-acoustic method: (a) $8^{th}$ vibration mode for Section 1; (b) $4^{th}$ vibration mode for Section 2; (c) $6^{th}$ vibration mode for Section 3; (d) $10^{th}$ vibration mode for Section 4.

# 4 Guided-Wave Ultrasonic SHM

The principle behind the guided-wave approach adopted here is quite simple. An actuator is used to launch an ultrasonic wave which is then sensed at a different point on the structure. A feature extracted from the recorded wave profile is then used for novelty detection. If the feature shows a deviation from normal condition, the implication is that damage has occurred somewhere on the path between the actuator and sensor (assuming for the moment that the feature does not contain components due to wave reflections from any boundaries). This data-based approach to guided-wave SHM was first discussed in [17, 18]. If a network of actuators and sensors is present, a series of 'pitch-catch' pairs can be defined covering different paths within the structure. If a novelty index is associated with each path, there is the potential for damage localisation, based on observing which paths cause their associated novelty detector to fire. if many overlapping paths are considered and it is not possible to eliminate reflections from all the responses, the interpretation of the novelty indices may not be straightforward, but it may be possible to use a neural network to classify the damage location [19, 20]. One of the main issues associated with the approach concerns the number of transducers needed. If the material of the structure has high attenuation for the wave propagation, the propagation paths need to be quite short, or the necessary information will not carry between actuator and sensor and a great many transducers will be needed to cover the structure; a nice discussion of transducer density for guided-wave SHM can be found in [21]. One problem in inspecting composite structures like wind turbines is the high level of attenuation [22]. The problem is made worse by the fact that the smallest damage that can be detected using wave-based SHM is determined by the wavelength; shorter wavelengths give better damage resolution, but they are attenuated more. On a composite structure like a wind turbine blade, which may be up to 100 m in length, the question of attenuation may determine whether ultrasonic wave-based SHM is feasible or not.

Part of the motivation for using the WT blade in the current study was to try and gain some insight into attenuation; although the blade is very short, it is composed of a material fairly typical in turbine blade manufacturing.

Following the first set of tests on the blade discussed in the previous section, a mistake in the experimental procedure for the guided-wave SHM was revealed, so a new blade was tested under both healthy and damaged conditions. Both sets of tests will be discussed here, because the mistake made in the first programme provided some useful insight into the wave propagation in the blade.

## 4.1 Experimental Procedure for the Guided Wave Test

In the first set of tests, the blade under investigation was the same blade that was subjected to the nonlinear acoustic testing. Seven pairs of piezoelectic transducers were bonded to the blade to actuate and sense signals; the placement of the sensors is shown schematically in Figure 13. The arrows in the figure show the actuator–sensor relationship for each pair of sensors. As discussed in the previous subsection, the object of the exercise was to use the actuator/sensor network to detect damage, and if possible, locate it, using the 'network of novelty detectors' approach [19, 20].

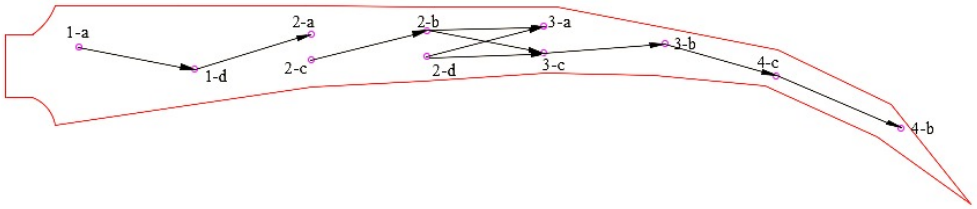


Figure 13: The arrangement of sensors and the Lamb wave propagation directions.

The experiment set up was the same as that described in Section 3.1. The high-frequency excitation signals needed were generated by the two-channel TTi-TGA 1242, 40 MHz arbitrary waveform generator and signal responses were acquired using the four-channel LeCroy Waverunner LT264, 350 MHz, 1 GS/s digital oscilloscope. The guided wave input signal was chosen to be a five-cycle sine wave toneburst with frequency 165 kHz and a peak-to-peak amplitude of 20 V modulated by a Hanning window. The response signal was sampled with a frequency of 500 MHz and computed from 15 averages. The thickness of the test blade is variable, and the geometry is complex, so guided waves were not expected to be Lamb waves. However, only one side of the blade was inspected and the actuators and sensors were placed close together in the seven pairs, so it was assumed that thickness was nearly constant over the wave propagation distances and that the waves could be approximated as Lamb waves. With these assumptions, the calculation of dispersion curves was obtained by reference to [23] and is illustrated in Figure 14.

As discussed above, the novelty detection approach depends on the extraction of multivariate features from the raw sensor data, which carry information about potential damage. In fact, previous work [17, 18, 19, 20] on guided-wave SHM, has shown that the necessary information is accessible in the time-domain response waveforms. If a wave passes through an area of damage, it experiences amplitude modulation, but also suffers phase changes (delays). In the case discussed here, the excitation frequency of the 'pitched' waveform was 165 kHz; each sampled waveform contained a 200 $\mu$s duration of data, and the interval between pulses was initially set at 10 ms. Each 'caught' (response) waveform contained 100000 sample points, and this represented huge redundancy in terms of information content; the dimension of a typical feature vector for machine learning is usually in the tens, so significant dimension reduction was needed. In the first case, only the first part of the response waveform was wanted as this would be the portion that has passed directly through the damage region without 'contamination' from reflections or waves that had passed around the diameter of the blade. A sampling window was used to eliminate boundary contamination signals, as shown in Figure 15.

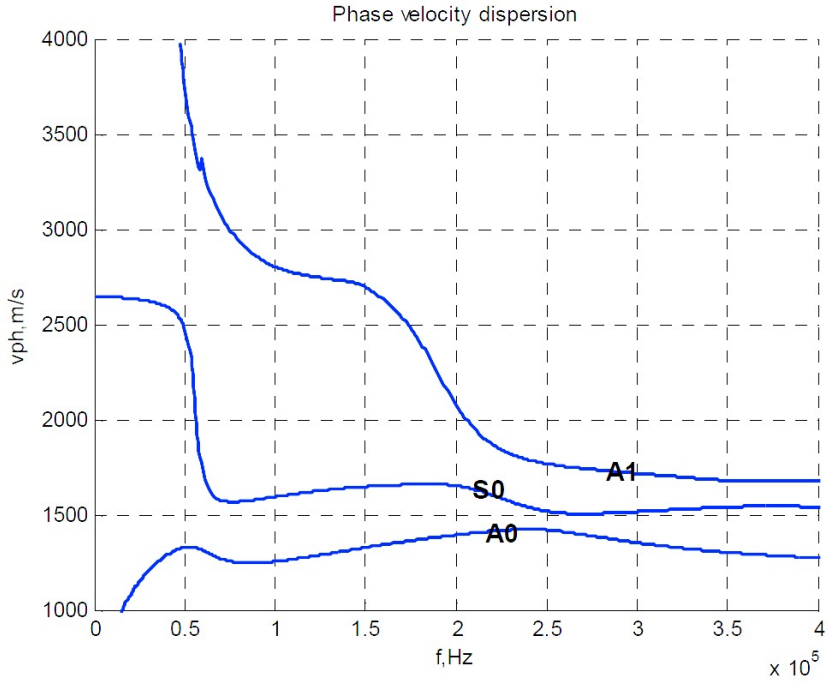


Figure 14: Dispersion curves for Glass Fibre Reinforced Plastic (GFRP) with 20 mm thickness [23].

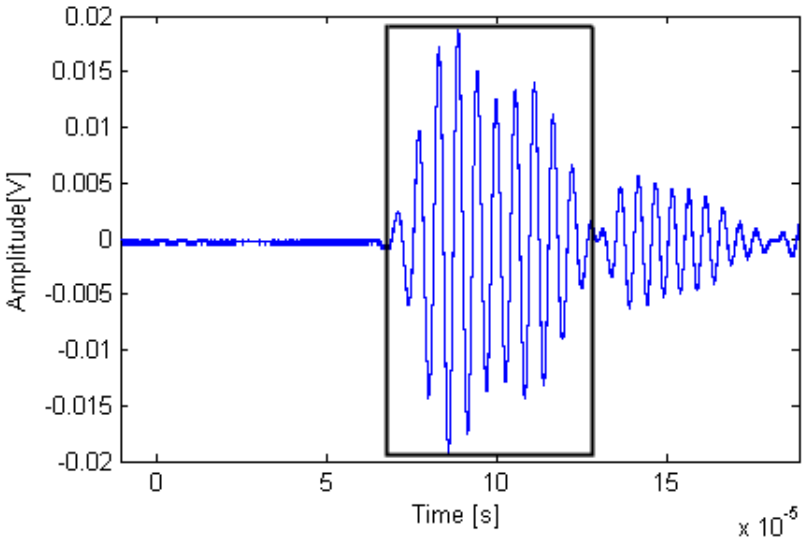


Figure 15: Outlier Analysis sampling window of guided wave response. The box shows the part of the overall record which was isolated for feature extraction. The first wavepacket was selected in order to remove contamination by boundary reflections etc. and to preserve the signal component which had passed directly through damage.

For the purposes of novelty detection, two sets of data were taken from the undamaged blade: 50 guided wave observations were taken as a 'training set' and a further 50 observations were chosen as a 'validation set'. Following the first impact – the imposition of damage – 50 additional observations were taken - the 'test set'. To recap, the location of the first impact damage introduced by the hammer is shown in Figure 8 (between sensor pairs 2-b and 3-c in Figure 13). As mentioned previously, there was no support underneath the strike area. In order to obtain appropriately low-dimensional features, the acquired waveforms were downsampled to give a 10-dimensional time-domain feature. This represents a very large reduction; however, previous

work had shown [17, 18, 19, 20] that such reductions still carry enough amplitude and phase information to produce damage-sensitive features. Once all the features were extracted, the novelty detection analysis could be carried out. In signal processing terms, the downsampling will have caused aliasing in the waveform feature; however, this was not considered a concern here, as the object of the exercise was simply novelty detection i.e. distinguishing between the features before and after damage.

## 4.2 Analysis and Results

The novelty detection technique applied to the data here was *outlier analysis* [24]; this is one of the simpler techniques possible, alternatives are discussed in [18]. The idea is based on a distance measure. One assumes that a set of feature vectors $\{\underline{x}_i; i = 1, \ldots, N\}$ are available as training data that represent the normal condition of the structure; in this case, the $\underline{x}_i$ are vectors of (downsampled) time data. The mean of this training set, $\overline{\underline{x}}$, is then estimated as a template for the normal condition (undamaged) state of the structure. For any subsequent monitored data, a weighted distance measure can be computed from the undamaged template – the *Mahalanobis squared-distance* (MSD),

$$D_\zeta^2 = (\underline{x}_\zeta - \overline{\underline{x}})^T S^{-1} (\underline{x}_\zeta - \overline{\underline{x}}) \tag{5}$$

where $\underline{x}_\zeta$ is a test point, and $S$ is the sample covariance matrix for the training data [24]. A separate sample mean, sample covariance and MSD measure are computed for each wave propagation path considered. If the MSD measure is considered 'too high', then the test point is considered to be too far from the normal condition template and is judged to have come from a damage state of the structure. The question of how high is 'too high' is settled in a principled way, by computing a threshold as described in [24]. The threshold is calculated via a Monte Carlo procedure and depends on both the dimension of the feature vector and the number of points in the training set; different thresholds can be computed corresponding to different levels of statistical confidence. The 99% threshold value for a 50-observation, 10-dimensional problem was found to be 55.5 after 1000 Monte Carlo trials of the algorithm given in [24].

The results of the outlier analysis are summarised in Figure 16. This figure shows the MSD measure on the (50-observation) validation ('before impact') and test data ('after impact') for each actuator-sensor pair; the red horizontal line represents the 99% confidence threshold for detection. The first important observation is that all of the validation (undamaged state) points, fall below the threshold as required. The second, less welcome, observation, is that *all* of the test points are above threshold i.e. damage is detected between *all* actuator sensor pairs. Furthermore, detection is strongest for the actuator-sensor pairs near the root of the blade, pairs that do not, in fact, cover the expected damage area. There were two possible explanations for the results.

In terms of the strongest indications of damage being close to the root of the blade; this raised a concern about the way in which the damage was induced. Damage was introduced into the blade by a single impact of a heavy instrumented hammer near the centre of the blade (Figure 8). The blade was not supported from below during the damaging impact and, with hindsight, it was considered possible that this introduced damage near the root of the blade as well as the centre. The only way to mitigate the effects of this, would be to repeat the tests with a new blade.

The more interesting point, is that damage was detected between *all* actuator sensor pairs, regardless of position. The explanation considered was as follows. As mentioned above, data were collected in sets of 50 observations, with each observation comprising a 15-signal average. This set of pulses were separated from each other by a 10 ms interval, so the tests took an overall time of 7.5 seconds. One reason why damage might be detected everywhere, is if the interval of 10 ms is too short; if the wave energy from previous pulses travels all around the blade and persists between data samples, then the wave profiles recorded between any actuator-sensor pair will contain a component from a wave that has passed through the damage. What is essentially happening is that the damage is being detected in the *diffuse field*. If one inspects Figure 16 closely, one can see that the novelty index increases steadily over the segments of validation data; this indicates that the normal condition profiles are actually changing over the test period, and

this supports the conclusion that the waves actually persist in the structure for a long period, and travel up and down the structure many times. Despite the failure of the test to meet its intended objectives, it has supplied evidence that there is very low wave attenuation in the blade; this in turn suggests that guided-wave SHM might be feasible with a low transducer-density network.

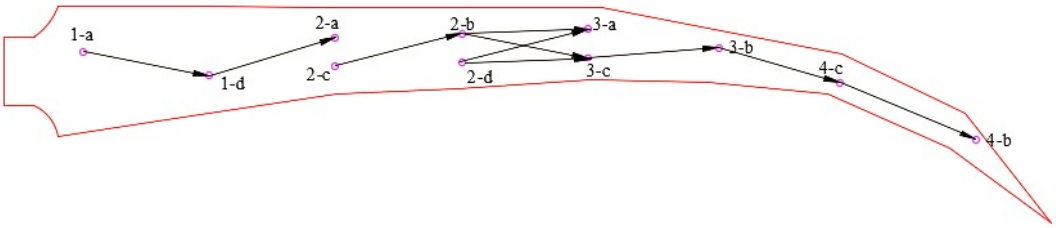


Figure 16: Outlier analysis classification results for the first impact test ('1a1d', '1d2a', '2c2b', '3c3b', '3b4c' and '4c4b' indicate sensor groups with reference to Figure 13).

Although a valuable lesson was learned from the first set of guided-wave tests, and the primary objective of detecting damage was successful, the secondary objective – of locating the damage – failed. With this in mind, a second series of tests were conducted using a nominally identical wind turbine blade to the first (the blades were originally purchased from the manufacturer in a batch of nine). The test and analysis procedures were identical to the earlier ones, except in three important respects. First, following the tests on the undamaged blade, damage was imposed in a slightly more careful manner. As before, the damage was caused by a hammer strike to the centre of the blade; however, this time, the blade was supported from below by a substantial steel rod. This meant that the hammer blow did not cause any bending at the blade root. There is a possibility that some damage was introduced into the bottom surface of the blade by the steel rod, but it was considered that this was unlikely to affect the overall damage location analysis. The second impact force was recorded with a maximum of 2082 N. The second change to the test procedure was to increase the interval between excitation pulses to 2 seconds. Although this increased the test durations by a factor of 50, this was considered essential in allowing the wave field to decay between pulses. Finally, the number of sensor actuator pairs in the vicinity of the damage was increased to four (see Figure 17).

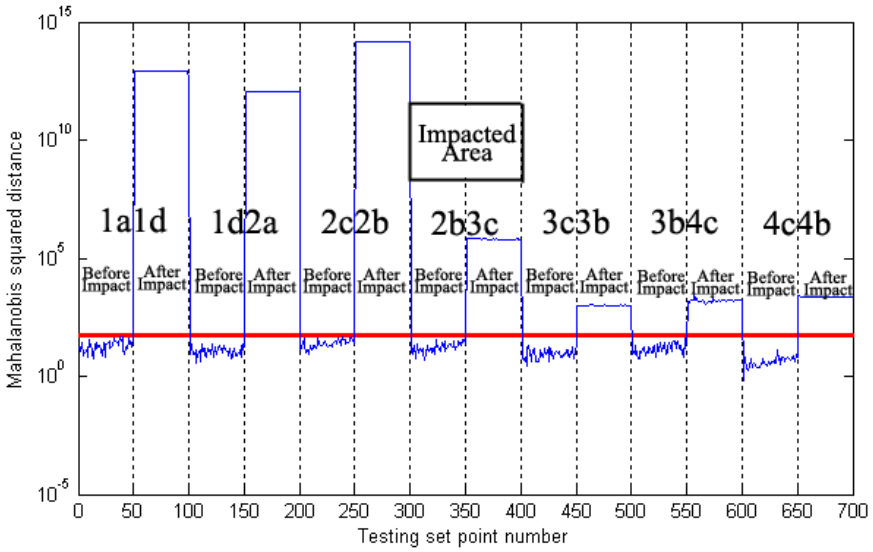


Figure 17: The arrangement of sensors and the Lamb wave propagation directions.

Data were acquired exactly as before with 50 averaged observations in the training, validation and test sets. The results of the outlier analysis are shown in Figure 18. This time, the procedure

shows complete success, both for detection and location. All the validation points are below threshold as required; furthermore, the MSD values for all actuator-sensor pairs which do not cover the damaged region are also below threshold. The MSD values for all actuator-sensor pairs that do cover the damage are all substantially above threshold (note the logarithmic vertical axis in Figure Figure 18). The methodology has thus detected and located the damage unambiguously. Finally, it is important to observe that the trends in the validation results, most visible in the 'Before impact' portions of Figure 16, are now absent. This is because the increased interval between actuation pulses is allowing the wavefield to decay between observations.

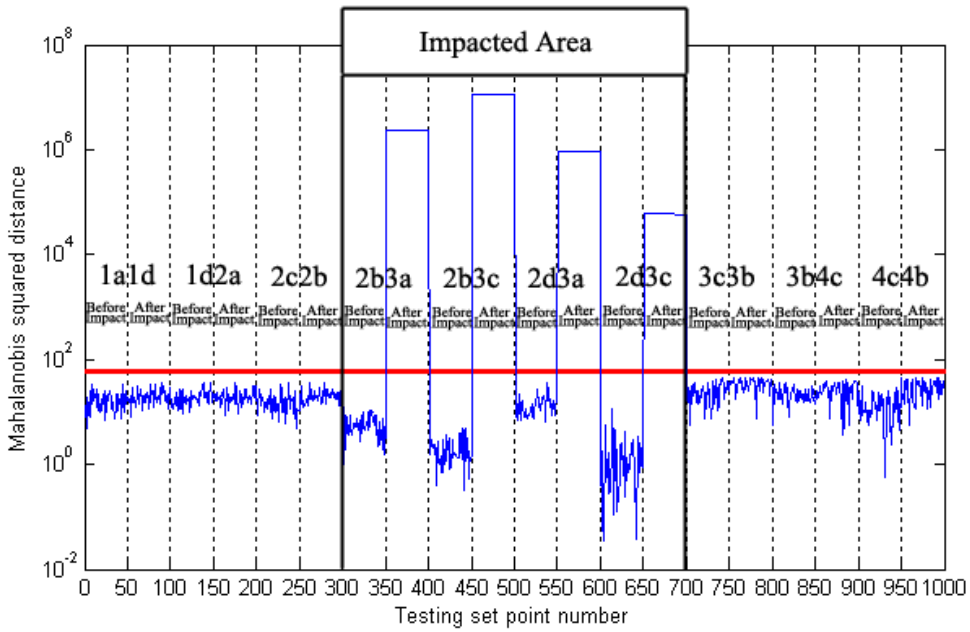


Figure 18: Outlier analysis classification results for the second impact test ('1a1d', '1d2a', '2c2b', '3c3b', '3b4c' and '4c4b' indicate sensor groups with reference to Figure 17).

# 5 Conclusions

This paper has presented a case study on the use of ultrasonic wave-based SHM for detecting and locating impact damage on a real (but small) wind turbine blade. Two techniques were applied: (i) nonlinear acoustics, and (ii) guided-wave SHM.

In the first case, the nonlinear acoustics approach was disappointingly insensitive to the damage. Analysis based on second-harmonic generation only detected the damage in one of four scenarios; a low/high-frequency vibro-acoustic approach failed to detect in any of the scenarios considered. This was partly unanticipated, given that the methods had successfully detected fatigue cracks in glass and aluminium coupons in previous tests. However, it had to be recognised that the WT blade considered here was considerably larger and more geometrically complicated than the plate specimens used in the previous tests. The likely cause of the failure is the fact that the stack actuator geometry which proved effective in previous studies in the coupons could not provide the necessary power to actuate the larger structure. It was noted that the single successful detection occurred when the stack actuator closest to the damaged area was used. If the actuation is indeed the issue, the prospects for using nonlinear acoustics on large-scale turbine blades appear to be rather dim. If damage can only be detected if an actuator is very close to the damage area, any practical system would require infeasible actuator densities. Furthermore, a real turbine monitoring system could not allow stack geometries which extend substantially out of plane, for aerodynamic reasons among others.

In contrast to the nonlinear acoustics approach, the guided-wave 'pitch-catch' approach was considerably more successful in detecting and locating the damage via a 'network of novelty

detectors' methodology. An initial experiment, which proved to be ill-conceived in two important respects, nonetheless showed that the approach could detect damage and also provided further interesting information. The first experiment showed that the attenuation experienced by the waves in the structure was quite low. This is a very important conclusion for the purposes of guided-wave SHM; if the waves can travel large distances, and still carry information about damage encountered in their path, then the possibility of low-density actuator-sensor networks for guided-wave SHM of WT blades is supported. Furthermore, the actuators for the guided-wave approach have a much lower profile than the stack actuators; although issues of power supply to transducers are still of major concern to wind turbine manufacturers and operators. Once the problems in the first experiment were corrected in the second, the guided-wave approach was able to detect and locate the damage, using a network of novelty detectors strategy. Of course, the results here are still not conclusive; the blade considered here is much smaller than most operational blades in use; however, it is realistic in terms of the composite material of its manufacture.

## Acknowledgements

KW would like to gratefully acknowledge the support of the UK Engineering and Physical Sciences Research Council (EPSRC) through grant reference numbers EP/J016942/1 and EP/K003836/2. KY acknowledges the support of Professor Wieslaw Staszewski (now of AGH University, Krakow, Poland) for his supervision and guidance in the early stages of his PhD project, and for setting the main objectives of that project. The authors would all like to thank Dr Evangelos (Vaggelis) Papatheou (now of the University of Exeter, UK) for his support in carrying out, and understanding, the modal tests on the wind turbine blade.

## References

[1] K. Yang. *Comparative Study of Nonlinear Acoustic and Guided Wave Methods for Structural Damage Detection*. PhD thesis, Department of Mechanical Engineering, University of Sheffield, 2014.

[2] K. Yang, K. Worden, and J.A. Rongong. Damage detection in a carbon fibre reinforced polymer (CFRP) plate using outlier analysis. In *Proceedings of International Conference on Damage Assessment – DAMAS 2013, Dublin, Eire*.

[3] K. Yang, K. Worden, J.A. Rongong, A. Hodzic, and A.D. Lafferty. Damage detection in a carbon fibre reinforced polymer (CFRP) plate using outlier analysis. In *Proceedings of International Conference on Advances in Mechanical and Manufacturing Engineering (ICAM2E), Kuala Lumpur, Malaysia*.

[4] National Research Council. Structural integrity of offshore wind turbines: Oversight of design, fabrication, and installation. Technical Report Special Report 305, The National Academies Press, Washington DC,, 2011.

[5] P. Brondsted and R.P.L. Nijssen. *Advances in Wind Turbine Blade Design and Materials*. Woodhead Publishing Limited, 2013.

[6] D. Wood. *Small Wind Turbines: Analysis, Design, and Application*. Springer, 2011.

[7] A.R. Jha. *Wind Turbine Technology*. CRC Press, 2010.

[8] T.W. Verbruggen. Wind turbine operation & maintenance based on condition monitoring. Technical Report ECN-C-03-047, Energy Research Centre of the Netherlands, 2003.

[9] A. Hikata, B.B. Chick, and C. Elbaum. Dislocation contribution to the second harmonic generation of ultrasonic waves. *Journal of Applied Physics*, 36:229–236, 1965.

[10] K.-Y. Jhang. Nonlinear ultrasonic techniques for nondestructive assessment of micro damage in material: A review. *International Journal of Precision Engineering and Manufacturing*, 10:123–135, 2009.

[11] D. Donskoy, A. Sutin, and A. Akimov. Nonlinear acoustic interaction on contact interfaces and its use for nondestructive testing. *NDT & E International*, 34:231–238, 2001.

[12] A. Klepka, W.J. Staszewski, R.b. Jenal, M. Szwedo, T. Uhl, and J. Iwaniec. Nonlinear acoustics for fatigue crack detection experimental investigations of vibro-acoustic wave modulation. *Structural Health Monitoring*.

[13] A. Klepka, W.J. Staszewski, D.d. Maio, and F. Scarpa. Impact damage detection in composite chiral sandwich panels using nonlinear vibro-acoustic modulations. *Smart Materials and Structures*, 22:084011, 2013.

[14] K.E.A. van den Abeele. Elastic pulsed wave propagation in media with second- or higher-order nonlinearity. Part I. Theoretical framework. *The Journal of the Acoustical Society of America*, 99:3334–3345, 1996.

[15] J.L. Devore and K.N. Berk. *Modern Mathematical Statistics with Applications*. Springer, 2012.

[16] J.L. Devore. *Probability and Statistics for Engineering and the Sciences*. Cengage Learning, Inc., eighth edition, 2010.

[17] W.J. Staszewski, S.G. Pierce, K. Worden, W.R. Philp, G.R. Tomlinson, and B. Culshaw. Wavelet signal processing for enhanced lamb wave defect detection in composite plates using optical fibre detection. *Optical Engineering*, 36:1877–1888, 1997.

[18] K. Worden, S.G. Pierce, G. Manson, W.R. Philp, W.J. Staszewski, and B. Culshaw. Detection of defects in composite plates using Lamb waves and novelty detection. *International Journal of System Science*, 31:1397–1409, 2000.

[19] F. Mustapha, G. Manson, K. Worden, and S.G. Pierce. Damage location in an isotropic plate using a vector of novelty indices. *Mechanical Systems and Signal Processing*, 21:1885–1906, 2007.

[20] D. Chetwynd, F. Mustapha, K. Worden, J.A. Rongong, S.G. Pierce, and J.M. Dulieu-Barton. Damage localisation in a stiffened composite panel. *Strain*, 44:298–307, 2008.

[21] A.J. Croxford, P.D. Wilcox, B.W. Drinkwater, and G. Konstantinidis. Strategies for guided-wave structural health monitoring. *Proceedings of the Royal Society of London A: Mathematical, Physical and Engineering Sciences*, 463:2961–2981, 2007.

[22] Z. Su, L. He, and Y. Lu. Guided Lamb waves for identification of damage in composite structures: a review. *Journal of Sound and Vibration*, 295:753–780, 2006.

[23] R. Raisutsis, E. Jasiuniene, and E. Zukauskas. Ultrasonic NDT of wind turbine blades using guided waves. *Ultrasound*, 63.

[24] K. Worden, G. Manson, and N.R. Fieller. Damage detection using outlier analysis. *Journal of Sound and Vibration*, 229:647–667, 1999.